JOURNAL OF SOLID STATE CHEMISTRY 57, 332–337 (1985)

Energy Transfer between Eu^{2+} Ions in $RbMgF_3$ Crystals

ALI M. GHAZZAWI, GEORGE E. VENIKOUAS, AND RICHARD C. POWELL

Physics Department, Oklahoma State University, Stillwater, Oklahoma 74078

Received July 30, 1984

Time-resolved spectroscopy after pulsed nitrogen laser excitation was used to characterize the energy transfer between Eu^{2+} ions in different crystal field sites in $RbMgF_3$ crystals. The results are consistent with electric dipole–dipole interaction and indicate that the Eu^{2+} ions are forming clusters in this host. As temperature is raised, the upper crystal field components of the metastable states of the ions become thermally populated and this changes the characteristics of the transfer process.

I. Introduction

The fluorescence properties of divalent europium ions in various host materials have been studied extensively for many years (*1, 2*). The two major reasons for the interest in this ion are its practical application as an X-ray intensifying phosphor and the fact that its spectral properties are highly sensitive to its local surroundings. This latter property makes Eu^{2+} an excellent probe of local crystal fields in different hosts. Recently there has been a significant amount of interest in characterizing the defect structure of doped alkali halide crystals. Ions such as Eu^{2+} and Mn^{2+} have been used to study the effects of charge compensation, impurity aggregation, and precipitation of impurity phases(*3, 7*). It has been shown that the defect structure affects many of the important physical properties of these crystals. This type of work is now being extended to other types of crystals such as $RbMgF_3$ (*8*).

In this paper we describe the results of a study of the fluorescence properties of Eu^{2+} ions in $RbMgF_3$ crystals using laser-excited, time-resolved, site-selection spectroscopy techniques. Emission of Eu^{2+} ions in different types of crystal field sites is identified and the energy transfer between ions in nonequivalent sites is characterized. The results clearly indicate that the Eu^{2+} ions are forming clusters in this host.

II. Experimental

Good optical quality single crystals were grown by the Bridgeman method in the Oklahoma State University Crystal Growth Facility. The sample investigated here contained about 0.05% Eu^{2+} and about 0.15% Mn^{2+}. A recent investigation of the optical properties of this sample has shown that the Eu^{2+} and Mn^{2+} ions tend to form pairs and that the excited Eu^{2+} ions in these pairs transfer virtually all of their energy to the Mn^{2+} ions (*8*). Therefore the Eu^{2+} ions which are paired with Mn^{2+} ions do not exhibit any fluorescence and the observed

0022-4596/85 $3.00

Eu^{2+} emission comes from ions which are not interacting with Mn^{2+}. This is verified by the fact that the measured Eu^{2+} fluorescence lifetime is not quenched by the addition of higher concentration of Mn^{2+} ions. Therefore in this study the presence of the Mn^{2+} ions in the crystal is essentially neglected since it does not affect the interaction between the Eu^{2+} ions which is the main focus of this paper.

The sample was mounted on the cold finger of a cryogenic refrigerator capable of varying the temperature between 10 K and 300 K. A Molectron UV-14 pulsed nitrogen laser was used as the excitation source. This produced a pulse of about 10 nsec in duration and 1 Å bandwidth at 3371 Å. The sample fluorescence was focused on the entrance slit of a 1-m Czerny–Turner monochromator set for a resolution of 0.03 nm. The signal was detected by an RCA C31034 photomultiplier tube, averaged by a PAR boxcar integrator, and recorded on a strip chart recorder. The time resolution of the system was set at 15 nsec.

The laser pulse excites the $^8S_{7/2}$–$^6P_{7/2}$ transition within the $4f^7$ configuration of Eu^{2+}. The inverse of this transition is the origin of the fluorescence emission in this host.

III. Low Temperature Results

Figure 1 shows the fluorescence emission of the Eu^{2+} ions at 12 K at two times after the laser pulse. There appears to be two dominant spectral lines with some less intense structure. The strong line at 3605.4 Å is the most intense at short times and the strong line at 3613.8 Å is the most intense at long times. Both of these lines are attributed to the same transition of Eu^{2+} ions in slightly different crystal field sites which have different energy level splittings. The ground state splitting (0.2 cm^{-1}) is too small to be observed and the weak structure on

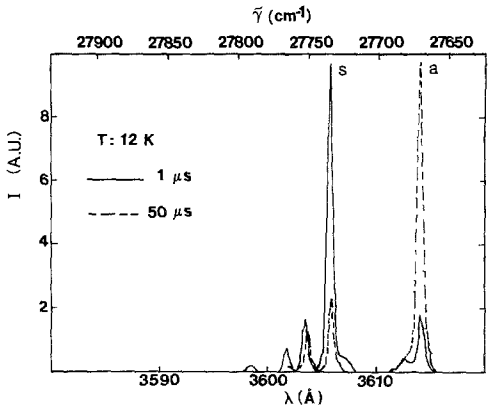

FIG. 1. Eu^{2+} emission spectra at 12 K at two times after the excitation pulse.

the higher energy side of each of the main lines is due to transitions from the higher crystal field multiplets of the $^6P_{7/2}$ level and ions in other less populated types of crystal field sites. The observed time dependence indicates that energy transfer is taking place from ions giving rise to the high energy line to ions in sites producing the low energy line. Thus these lines are labeled sensitizer (S) and activator (A), respectively. The lifetime of the former is measured to be 50.09 μsec and that of the latter is 103.84 μsec. These are listed in Table I.

In order to quantitatively characterize the dynamics of the energy transfer process the ratio of the integrated intensities of the activator to the sensitizer lines was plotted versus time after the laser pulse as shown in Fig. 2. There is a rapid increase at short times and then a leveling off at longer times indicating some equilibrium condition has been reached.

In order to interpret these energy transfer data a model involving the interaction of two two-level systems is assumed as shown in Fig. 3. The rate equations describing the dynamics of the excited state populations are

$$dn_s(t)/dt = n_s(0)\delta(t) - (\beta_s + W_{sa})n_s(t) + W_{as}n_a(t) \quad (1)$$

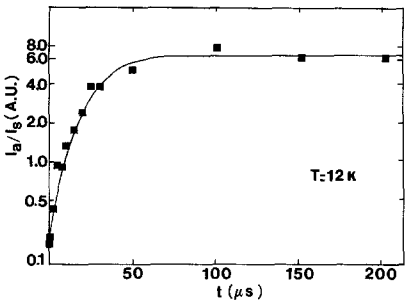

FIG. 2. Ratios of the integrated fluorescence intensities as a function of time after the exciton pulse at 12 K. See text for explanation of the theoretical line.

$$dn_a(t)/dt = n_a(0)\delta(t) - (\beta_a + W_{as})n_a(t) + W_{sa}n_s(t) \quad (2)$$

where $n_s(t)$ and $n_a(t)$ are the populations of the excited states of sensitizers and activators at time t, respectively, β_s and β_a are the fluorescence decay rates of the ions in the two types of sites, and W_{sa} and W_{as} are the energy transfer and back transfer rates. The excitation pulse is approximated by a $\delta(t)$ function. The excited state populations are related to the measured fluorescence intensities by $I_i = \beta_i^r n_i$ where β_i^r represents the radiative decay rate. The solution to these equations gives

$$I_a(t)/I_s(t) = [I_a(0)/I_s(0)]\{1 + G_a\tanh(Bt)\}/\{1 + G_s\tanh(Bt)\} \quad (3)$$

where

$$B^2 = \tfrac{1}{4}[W_{sa} + \beta_s - W_{as} - \beta_a)^2 + W_{sa}W_{as}$$

$$G_a = \{[n_s(0)/n_a(0)]W_{sa} + \tfrac{1}{2}(W_{sa} + \beta_s - W_{as} - \beta_a)\}/B$$

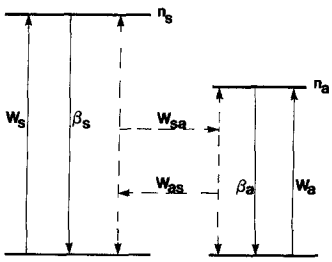

FIG. 3. Two-level system model for energy transfer.

$$G_s = \{[n_a(0)/n_s(0)]W_{as} - \tfrac{1}{2}(W_{sa} + \beta_s - W_{as} - \beta_a)\}/B.$$

The solid line in Fig. 2 represents the best fit to the data obtained from Eq. (3) treating the energy transfer rates, the initial population ratio, and the ratio of radiative lifetimes as adjustable parameters. The values of these parameters are listed in Table I.

IV. Results at Higher Temperatures

As temperature is raised, the Eu^{2+} emission spectrum becomes much more complex. This is due partially to emission from thermally populated upper components of the crystal field split manifold of the metastable state. In addition, the population of new levels and the presence of thermal energy cause the activation of energy transfer to Eu^{2+} ions in new types of sites. A portion of the emission spectrum at 77 K is shown in Fig. 4 at two times after the excitation pulse. The sensitizer line at 3605.4 Å still is strongly selectively excited but now emission can also be observed from the next higher crystal field component of the meta-

TABLE I

ENERGY TRANSFER PARAMETERS

	T (K)	
Parameter	12	77
τ_s (μsec)	50.1	20.7
τ_a (μsec)	103.8	693.0
W_{sa} (sec^{-1})	6.16×10^4	
W_{as} (sec^{-1})	0.90×10^4	
$n_a(0)/n_s(0)$	0.25	
β_s^r/β_a^r	1.15	
R_0 (Å)	7.8	9.0
R_{sa} (Å)	6.5	9.0
τ_r (μsec)	50.1	
W_t^{-1} (μsec)	15.4	
W_p^{-1} (msec)	1.0	
ΔE_t (cm^{-1})	31.25	
ΔE_p (cm^{-1})	34.27	

Note. Values below broken line obtained from temperature dependent data.

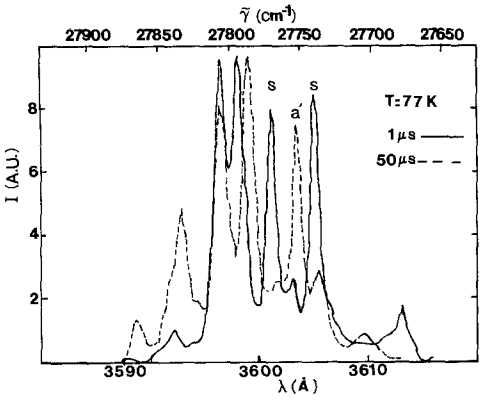

FIG. 4. Eu^{2+} emission spectra at 77 K at two times after the excitation pulse.

stable state of the ions in this type of site. This appears as the line at 3601.2 Å in the spectrum which implies a crystal field splitting of $\delta E = 32.4$ cm^{-1}. The activator line identified at low temperature is weak and shows little relative time dependence at high temperatures. This indicates that the ions in this type of site are no longer effective in receiving the energy from the ions in the sensitizer sites. Instead, the relative time evolution of the spectral line at 3603.0 Å indicates that the ions in the type of site producing this transition are being strongly pumped through energy transfer from the sensitizer ions. Although some of the spectral lines at higher energy may be associated with other transitions from these activator ions, the overlap among the various lines makes it impossible to make any conclusive assignment.

The general form of the time dependence of the ratio of the integrated intensities of the sensitizer and activator transitions is similar to that observed at low temperatures. No attempt was made to quantitatively fit the high temperature time-resolved spectroscopy data with a two-level system model since the complex nature of the spectrum does not allow the lines to be resolved cleanly. Thus the error bars on the data were too large to obtain unique theoretical fits.

The evolution of the spectral characteristics with temperature from the 12 K to the 77 K values is very complex because of the presence of various different types of physical processes. For example, Fig. 5 shows the change with temperature of the ratio of the integrated fluorescence intensities of the sensitizer and the activator emissions at 1 μsec after the excitation pulse. There is no point below 20 K because no emission from this type of activator can be observed at these temperatures. The high value of the ratio at low temperature is due to the quenching of the sensitizer fluorescence by energy transfer to the low temperature type of activator ions. The ratio decreases as temperature is increased because this type of process is turning off.

Figure 6 shows the changes in the fluorescence lifetimes with temperature. The low temperature activator emission quenches rapidly with temperature whereas the sensitizer emission decreases rapidly at low temperature and begins to level out at high temperature. The high temperature activator emission exhibits a more complex behavior with a very rapid decrease at low

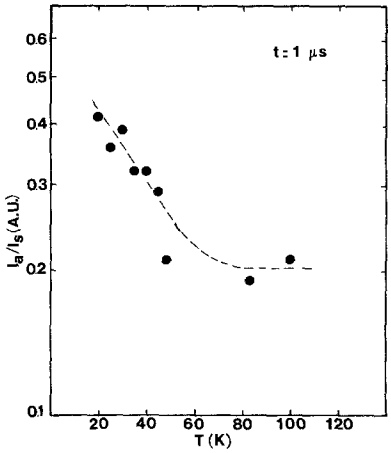

FIG. 5. Temperature dependences of the fluorescence intensity ratios taken at 1.0 μsec after the excitation pulse.

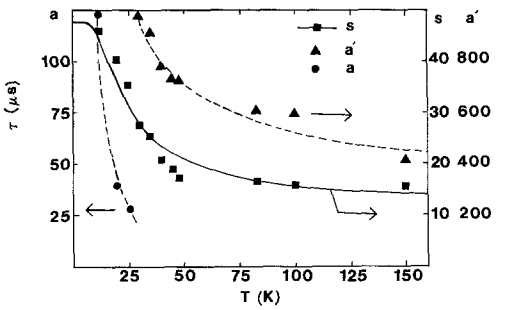

FIG. 6. Temperature dependences of the fluorescence lifetimes of the sensitizer (s), low temperature activator (a), and high temperature activator (a') ions. See text for explanation of the theoretical line.

temperatures, a less rapid decrease between 50 and 100 K, and then a more rapid decrease at higher temperatures. These changes again indicate the occurrence of complex spectral dynamics. An example of one possible way to interpret the temperature variation of the sensitizer decay time is through the equation

$$\tau_f^{-1} = \tau_r^{-1} + W_t \exp[-\Delta E_t/kT] + W_p\{1 - \exp[-\Delta E_p/kT]\}^{-1}. \quad (4)$$

Here τ_f is the fluorescence decay time of these ions, τ_r is the radiative decay time, W_t is the energy transfer rate, and W_p is the phonon emission rate. The transfer process is assumed to occur with an exponential activation energy of ΔE_t. The phonon emission term was needed in order to obtain the leveling off of the lifetime at high temperatures. The solid line in the figure represents the best fit to the data using Eq. (4) and treating the various rates and activation energies as adjustable parameters. The parameters obtained in this way are listed in Table I.

V. Discussion and Conclusions

At 12 K the best fit to the time-resolved spectroscopy data was obtained using a time-independent energy transfer rate. Attempts to obtain a good fit to the data with time-dependent rates were unsuccessful. Constant energy transfer rates indicate the presence of one of two possible physical situations. The first is transfer over fixed sensitizer–activator separations and the second is transfer involving efficient migration of energy among the sensitizer ions before transfer to activators. The latter process is unlikely in this case because of the low concentration of sensitizer ions.

For constant sensitizer–activator separation R_{sa}, the energy transfer rate for electric dipole–dipole interaction can be expressed as

$$W_{sa} = \tau_s^{-1}(R_0/R_{sa})^6 \quad (5)$$

where the critical interaction distance R_0 is given by (9)

$$R_0 = \{\tfrac{3}{4}[e^2/mc^2][\Omega\phi_s f_a]/(2\pi n\nu_{sa})^4\}^{1/6}. \quad (6)$$

Here n is the index of refraction for $RbMgF_3$, ν_{sa} is the average wavenumber in the region of spectral overlap, ϕ_s is the quantum efficiency of the sensitizer, f_a is the oscillator strength of the activator transition, and Ω is the spectral overlap integral for the sensitizer and activator transitions. The latter two quantities can be found from

$$\Omega = \pi^{-1}[\Delta\upsilon_s + \Delta\upsilon_a]/[(\Delta\upsilon_s + \Delta\upsilon_a)^2 + (\upsilon - \upsilon_a)^2]$$

and

$$f_a = (1.51)\tau_a^{-1}\lambda_a^2[(n^2 + 2)/3)^2 n]^{-1}$$

where υ_i and $\Delta\upsilon_i$ are the positions and widths of the spectral transitions. Using observed spectral parameters, the critical interaction distance is predicted to be 7.8 Å at 12 K and 9.0 Å at 77 K. If these values are substituted into Eq. (5) along with the measured fluorescence lifetimes and the energy transfer rates obtained respectively from fitting the time-resolved spectroscopy and fluorescence lifetime temperature variation data, the sensitizer–activator separations are found to be approximately 6.5 Å at 12 K and 9.0 Å at 77 K. X-ray crystal structure

results show the nearest neighbor separation between two Eu^{2+} sites to be 5.84 Å and the fifth nearest neighbor separation to be 9.6 Å in $RbMgF_3$ crystals (*10*). This shows that the energy transfer observed in this work occurs between Eu^{2+} ions in cluster formations.

Using Eq. (4) the transfer rate to the high temperature activator was found to be about 4.7×10^4 sec^{-1} at 77 K and the activation energy for this transfer is 31.2 cm^{-1}. The latter value is consistent with the measured splitting of 32.4 cm^{-1} between the two crystal field components of the sensitizer. The ratio of the back transfer to the transfer rate should be proportional to a Boltzmann factor $\exp\{-\Delta E_{sa}/kT\}$. The data obtained at 12 K predicts a value of $\Delta E_{sa} =$ 13.3 cm^{-1} which is close to the difference in the energies of the high energy activator level and the upper crystal field component of the sensitizer, 13.1 cm^{-1}.

In summary, these results show the complex nature of the dynamics of the interaction among clusters of Eu^{2+} ions occupying three different types of sites. The picture most consistent with all of the data is that the sensitizer transfers energy to the high energy activator from its upper crystal field state as it relaxes from the excited $^6P_{7/2}$ level. At low temperature this activator either transfers the energy on to the low temperature activator which fluoresces or back-transfers to the sensitizer, whereas at high temperature it either fluoresces itself or back-transfers. The transfer process is consistent with electric dipole–dipole interaction and is enhanced by the thermal occupation of the upper crystal field component of the sensitizer. The microscopic origin of the different types of sites is not known but is probably due to the presence of structural or chemical impurities in the lattice.

In conclusion, this work demonstrates the usefulness of time-resolved site-selection energy transfer studies to elucidate impurity ion distributions in host crystals. In particular, the results show that Eu^{2+} ions are forming close neighbor clusters in $RbMgF_3$ crystals even at very low concentrations.

Acknowledgments

We are grateful to M. D. Shinn and W. A. Sibley for helpful discussions concerning this work and for providing us with a copy of a preprint of their manuscript (Ref. (*8*)). In addition, we are grateful to J. J. Martin for growing the sample used in this work and to E. M. Holt for her X-ray crystal structure work on this material. This work was supported by National Science Foundation Grant DMR-82-16551.

References

1. G. Blasse and A. Bril, *Philips Tech. Rev.* **31,** 303 (1970).
2. L. H. Brixner, J. D. Bierlein, and V. Johnson, *in* "Current Topics in Materials Science" (E. Kaldis, Ed.), Vol. 4, p. 47, North-Holland, New York (1980).
3. J. Garcia-Sole, M. Aguilar G., F. Agullo-Lopez, H. Murrieta S., and J. Rubio O., *Phys. Rev. B* **26,** 3320 (1982).
4. F. J. Lopez, H. Murrieta S., J. Hernandez A., and J. Rubio O., *Phys. Rev. B* **22,** 6428 (1980).
5. F. Rodriguez, M. Moreno, F. Jaque, and F. J. Lopez, *J. Chem. Phys.* **78,** 73 (1983).
6. J. L. Pascual, L. Arizmendi, F. Jaque, and F. Agullo-Lopez, *J. Lumin.* **17,** 325 (1978).
7. L. D. Merkle, R. C. Powell, and T. M. Wilson, *J. Phys. C* **11,** 3103 (1978).
8. M. D. Shinn and W. A. Sibley, *Phys. Rev. B* **29,** 3834 (1984).
9. D. L. Dexter, *J. Chem. Phys.* **21,** 836 (1953).
10. E. M. Holt, unpublished results.